Electronic Supplementary Material (ESI) for Journal of Materials Chemistry C.

Eu(III) Functionalized HOFs Based on Machine-Learning-Assisted Fluorescence Sensing: Discrimination of Quinolones via PCA and BPNN Model

*Kai Zhu[a], Xin Xu[a] and Bing Yan[a]**

a School of Chemical Science and Engineering, Tongji University, Siping Road 1239, Shanghai 200092, China.

* Corresponding author: Email address: byan@tongji.edu.cn (Bing Yan)

Electronic supplementary information

Fig. S1. (a) Experimental PXRD patterns of Tb@HOF-GS-10 (blue line), Sm@HOF-GS-10 (green line), Dy@HOF-GS-10 (purple line) and simulated PXRD pattern (red line). (b) FT-IR spectra of HOF-GS-10 (red line), Tb@HOF-GS-10 (blue line), Sm@HOF-GS-10 (green line) and Dy@HOF-GS-10 (purple line).

Fig. S2. (a) XPS spectra of Eu 3d electron in $Eu(NO_3)\cdot 6H_2O$. (b) XPS spectra of Eu 3d electron in **1**. (c) XPS spectra of O1s in HOF-GS-10. (d) XPS spectra of O1s in **1**.

Fig. S3. (a) SEM picture of HOF-GS-10. (b) SEM picture of **1**.

Fig. S4. EDX mapping images of O, N and S elements respectively in HOF-GS-10.

Fig. S5. (a) The element content of C (48.40%), N (17.96%), O (17.51%) and S (16.14%) elements in EDX energy spectrum of HOF-GS-10. (b) The element content of C (33.14%), N (2.42%), O (21.51%), S (12.40%) and Eu (30.52%) elements in EDX energy spectrum of **1**.

Fig. S6. (a) Excitation spectrum and Emission spectra of 1,5-napthalenedisulfonic acid. (b) Excitation spectrum and Emission spectra of HOF-GS-10.

Fig. S7. (a) Excitation spectrum and Emission spectra of Tb@HOF-GS-10. (b) Excitation spectrum and Emission spectra of Sm@HOF-GS-10. (c) Excitation spectrum and Emission spectra of Dy@HOF-GS-10. (d) CIE chromaticity diagram obtained under excitation at 323 nm of **1** mixed with eight quinolones (QNs). The inset shows that **1** mixed with eight QNs is excited under 310 nm laboratory UV light. (The relative values of the CIE chromaticity diagram of **1** mixed with eight QNs are shown in Table S2.)

Fig. S8. (a) Dependence of emission intensity for **1** on temperature (10−50 ℃) upon λ_{ex} = 323 nm. (b) Histogram of emission intensity for **1** on temperature (10−50 ℃) upon λ_{ex} = 323 nm.

Fig. S9. Canonical 2D score plot for response patterns as obtained from PCA for ten QNs at 10^{-3} M. Ellipses represent 95% confidence.

Fig. S10. Luminescence intensity of 616 nm peak for **1** after four repetitions with 10^{-3} M eight QN solutions. (a) ciprofloxacin (CF), (b) flumequine (FQ), (c) gatifloxacin (GF), (d) levofloxacin (LF), (e) marbofloxacin (MF), (f) norfloxacin (NF), (g) ofloxacin (OF) and (h) pefloxacin (PF).

Fig. S11. Time-response emission spectra at 616 nm (excited at 323 nm) of **1** upon addition of 10^{-3} M eight QNs. (a) ciprofloxacin (CF): RT = 52 s, (b) flumequine (FQ): RT = 32 s, (c) gatifloxacin (GF): RT = 61 s, (d) levofloxacin (LF): RT = 79 s, (e) marbofloxacin (MF): RT = 26 s, (f) norfloxacin (NF): RT = 39 s, (g) ofloxacin (OF): RT = 47 s and (h) pefloxacin (PF): RT = 67 s. (RT: response time)

Fig. S12. The chemical structural formula of eight QNs.

Fig. S13. Schematic diagram for the fluorescence response of **1** toward QNs mechanism. (ISC: intersystem crossing; ET: energy transfer)

Fig. S14. Decay lifetimes of emission peak of 616 nm (Eu^{3+} $^5D_0 \rightarrow {}^7F_2$ transition) for **1** with 10^{-3} M eight QNs. (a) ciprofloxacin (CF), (b) flumequine (FQ), (c) gatifloxacin (GF), (d) levofloxacin (LF), (e) marbofloxacin (MF), (f) norfloxacin (NF), (g) ofloxacin (OF) and (h) pefloxacin (PF).

Fig. S15. Canonical 2D score plot for response patterns as obtained from PCA for 10^{-3} M LF、GF and 1:1 mixture of LF and GF. Ellipses represent 95% confidence.

Fig. S16. Canonical 2D score plot for response patterns as obtained from PCA for eight QNs at 10^{-3} M in various components in (a) urine and (b) serum system (λ_{ex} = 323 nm). Ellipses represent 95% confidence.

Fig. S17. Network training curve of the BPNN. Horizontal axis: Epoch; Vertical axis: Training MSE

Fig. S18. Deviation curve of the BPNN (OV: original value; CV: calculated value). Horizontal axis: Eight concentrations of input items; Vertical axis: Training MSE.

Table S1. Element contents of C, N, O, S in EDX energy spectrum HOF-GS-10 and C, N, O, S, Eu in EDX energy spectrum **1**.

Table S2. The relative values of the CIE chromaticity diagram of **1** mixed with eight QNs.

Table S3. Summary of fluorescence sensing parameters of **1** for detecting eight QNs in ethanol System.

Table S4. Summary of the methods for sensing FQ.

Table S5. Summary of fluorescence decay lifetime of **1** in ethanol (ET), **1** powder and **1** mixed with eight QNs at 298 K.

Table S6. Summary of input and output information during the training of BPNN for GF concentrations detection.

Table S7. Network structure information.

Table S8 The summary of mean square error (MSE), original value (OV.), calculated value (CV.), variance (Var.).

Table S9. The summary of input and output information in real batch calculation during the test of BPNN.

Experimental Section

Materials and physical measurements

The PCA model was constructed by Orign 2021 program. The BPNN model was constructed in Maishi Neural Network program package. Ln@$(NO_3)_3 \cdot 6H_2O$ (Ln=Eu, Tb, Sm, Dy) was prepared by dissolving their oxides in excess hydrogen nitrate with continuous stirring, followed by evaporation and crystallization several times. All the other reagents and solvents employed were commercially available and used as received without further purification. Ultrapure water was used throughout all experiments. The power X-ray diffraction (PXRD) pattern was recorded via a Bruker D8 Advance diffractometer, with a scan range of 2 theta from 5 to 50°. Fourier transform infrared spectra (FT-IR) of powder samples were collected on a Nicolet IS10 infrared spectrum radiometer in the range of 4000 - 400 cm^{-1} using KBr slices. Scanning electron microscopy (SEM) and energy dispersive X-ray (EDX) analysis were performed on a Hitachi S-4800 field emission scanning electron microscope operating at 3 KV and 15 KV, respectively. X-ray photoelectron spectroscopy (XPS) spectra were recorded under ultrahigh vacuum ($<10^{-6}$ Pa) at a pass energy of 93.90 eV with an Axis Ultra DLD spectrometer (Kratos, Japan) by using an Mg Kα (1253.6 eV) anode. The excitation and emission spectra of the experimental samples were obtained on an Edinburgh FLS920 spectrophotometer with a xenon lamp (450 W) as an excitation source. Luminescence lifetime measurements were measured at room temperature on an Edinburgh FLS920 phosphorimeter using a microsecond lamp (100 mW). The corresponding Commission International de l'Eclairage (CIE) color coordinates were calculated on the basis of the international CIE standards.

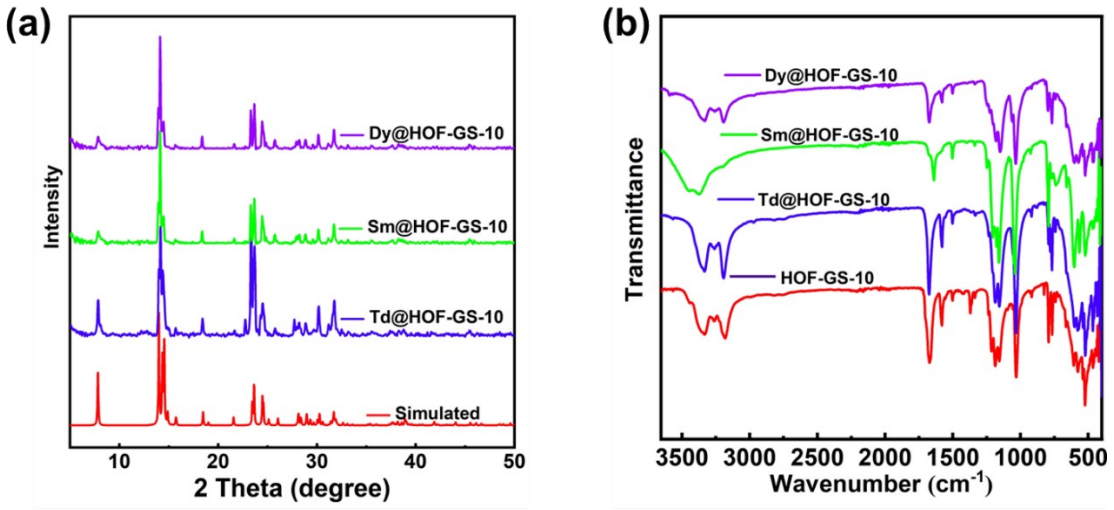

Fig. S1. (a) Experimental PXRD patterns of Tb@HOF-GS-10 (blue line), Sm@HOF-GS-10 (green line), Dy@HOF-GS-10 (purple line) and simulated PXRD pattern (red line). (b) FT-IR spectra of HOF-GS-10 (red line), Tb@HOF-GS-10 (blue line), Sm@HOF-GS-10 (green line), Dy@HOF-GS-10 (purple line).

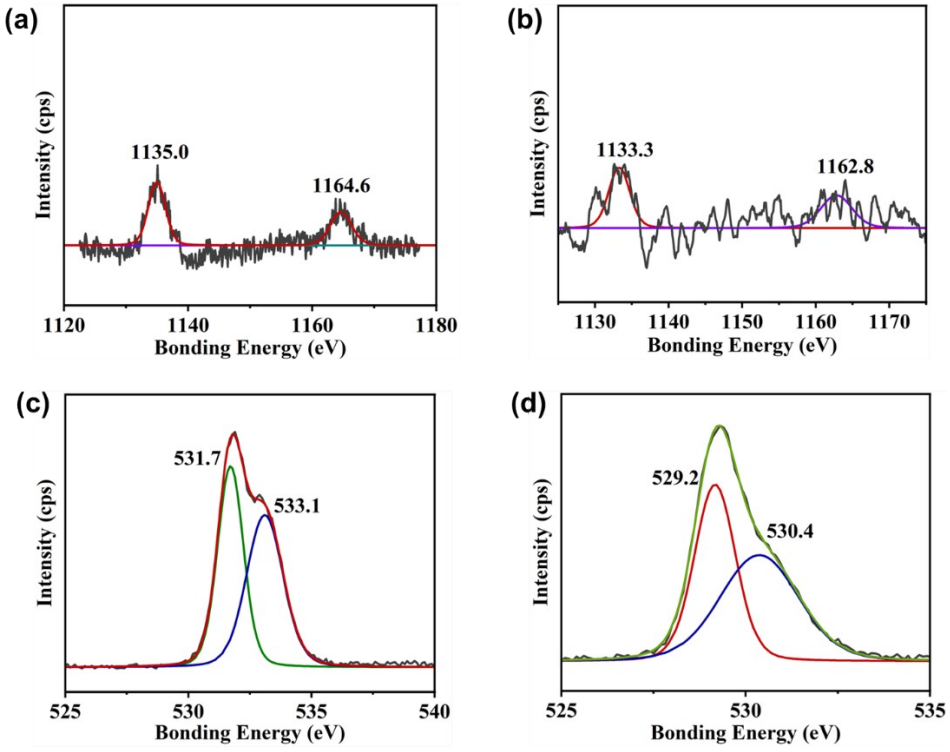

Fig. S2. (a) XPS spectra of Eu 3d electron in $Eu(NO_3)\cdot 6H_2O$. (b) XPS spectra of Eu 3d electron in **1**. (c) XPS spectra of O1s in HOF-GS-10. (d) XPS spectra of O1s in **1**.

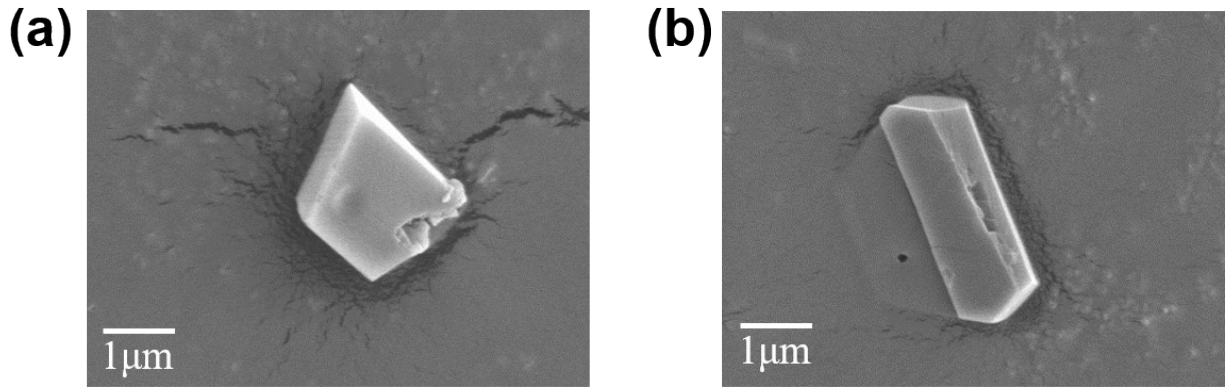

Fig. S3. (a) SEM picture of HOF-GS-10. (b) SEM picture of **1**.

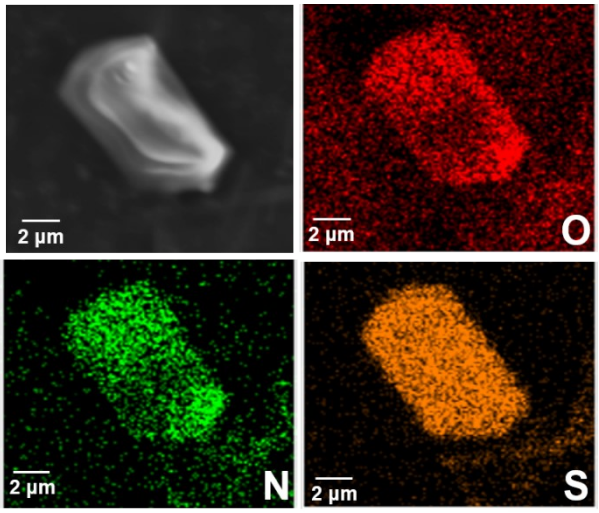

Fig. S4. EDX mapping images of O, N and S elements respectively in HOF-GS-10.

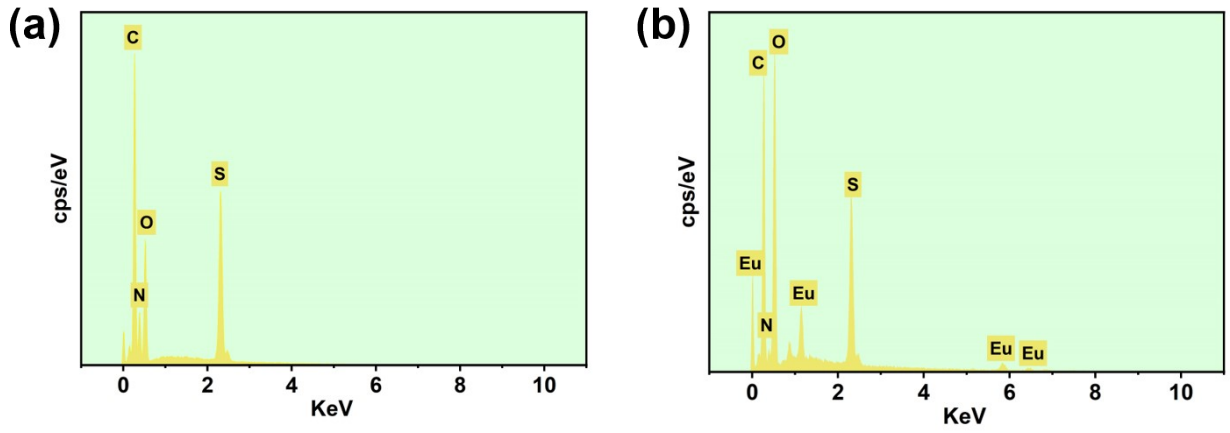

Fig. S5. (a) The element content of C (48.40%), N (17.96%), O (17.51%) and S (16.14%) elements in EDX energy spectrum of HOF-GS-10. (b) The element content of C (33.14%), N (2.42%), O (21.51%), S (12.40%) and Eu (30.52%) elements in EDX energy spectrum of **1**.

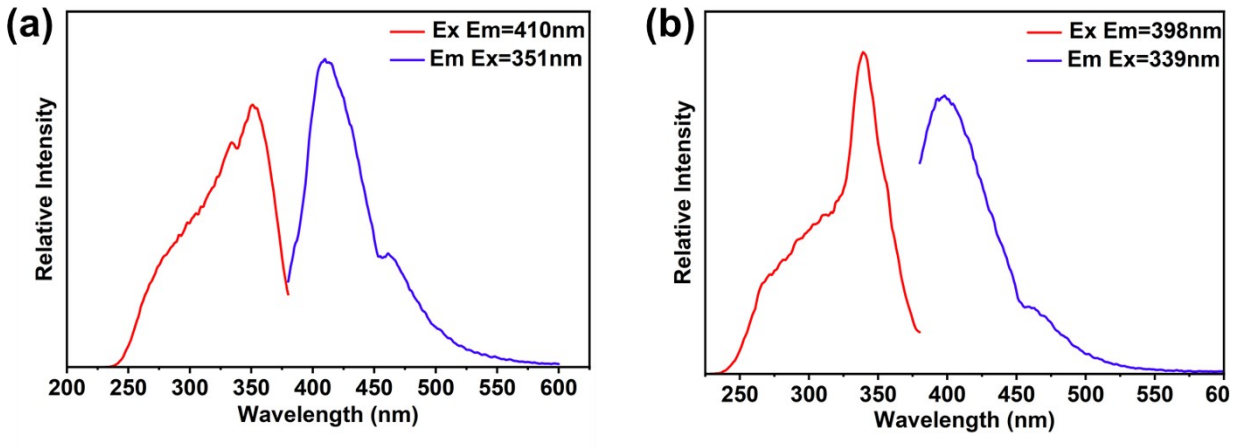

Fig. S6. (a) Excitation spectrum and Emission spectra of 1,5-napthalenedisulfonic acid. (b) Excitation spectrum and Emission spectra of HOF-GS-10.

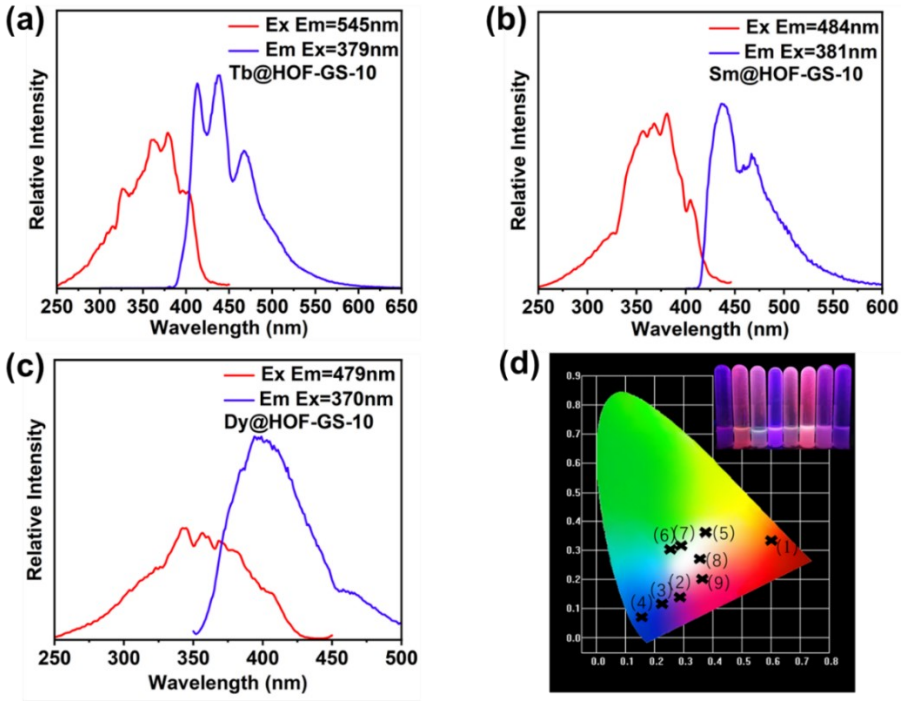

Fig. S7. (a) Excitation spectrum and Emission spectra of Tb@HOF-GS-10. (b) Excitation spectrum and Emission spectra of Sm@HOF-GS-10. (c) Excitation spectrum and Emission spectra of Dy@HOF-GS-10. (d) CIE chromaticity diagram obtained under excitation at 323 nm of **1** mixed with eight quinolones (QNs). The inset shows that **1** mixed with eight QNs is excited under 310 nm laboratory UV light. (The relative values of the CIE chromaticity diagram of **1** mixed with eight QNs are shown in Table S2.)

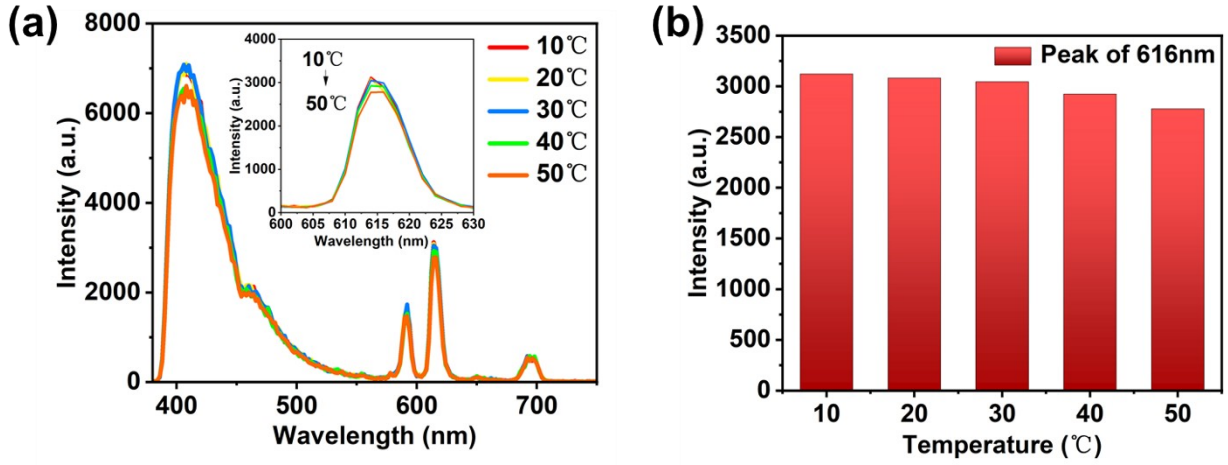

Fig. S8. (a) Dependence of emission intensity for **1** on temperature (10–50 ℃) upon λ_{ex} = 323 nm. (b) Histogram of emission intensity for **1** on temperature (10–50 ℃) upon λ_{ex} = 323 nm.

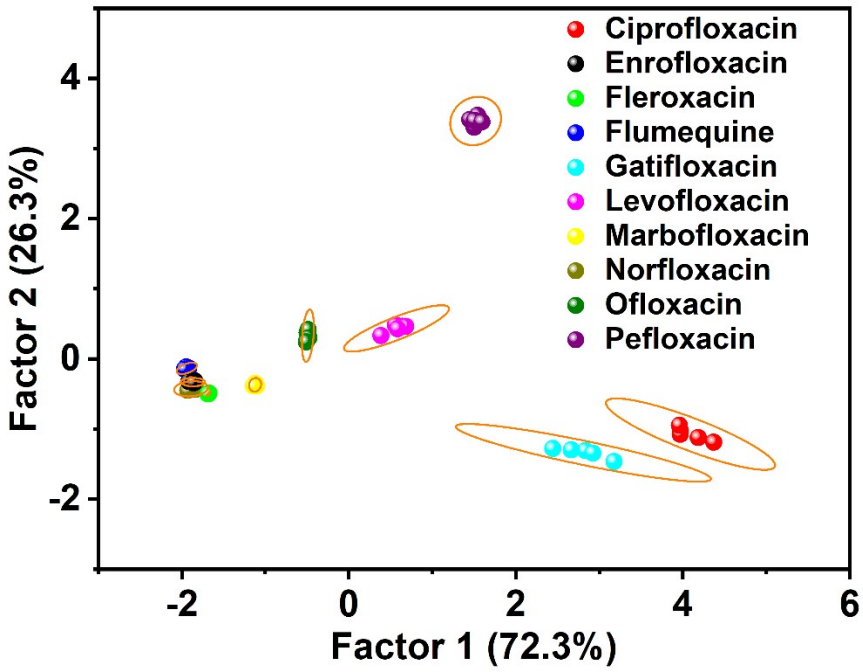

Fig. S9. Canonical 2D score plot for response patterns as obtained from PCA for ten QNs at 10^{-3} M. Ellipses represent 95% confidence.

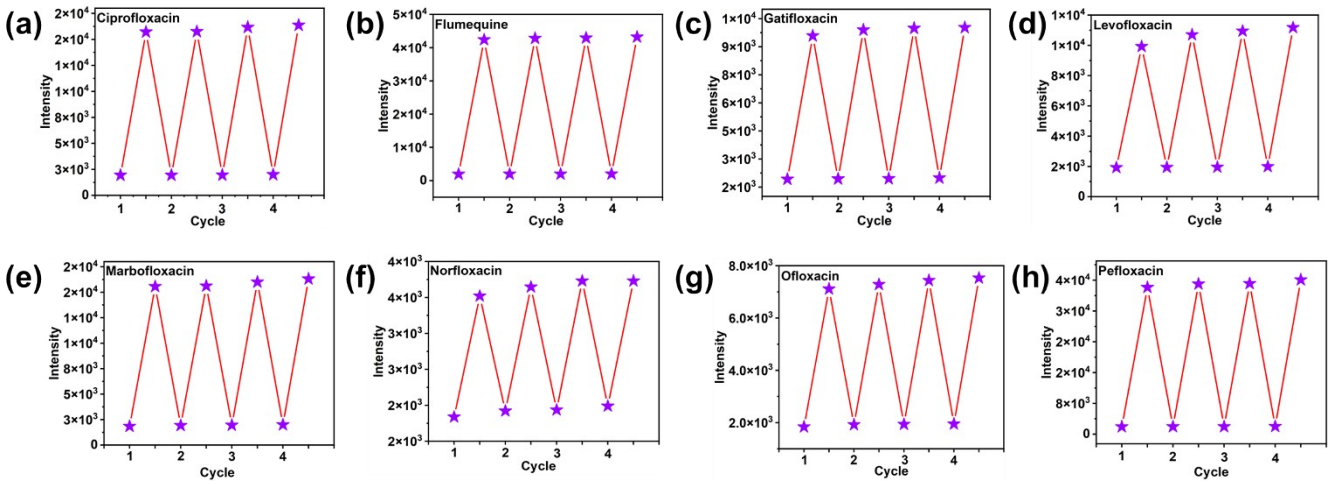

Fig. S10. Luminescence intensity of 616 nm peak for **1** after four repetitions with 10^{-3} M eight QN solutions. (a) ciprofloxacin (CF), (b) flumequine (FQ), (c) gatifloxacin (GF), (d) levofloxacin (LF), (e) marbofloxacin (MF), (f) norfloxacin (NF), (g) ofloxacin (OF) and (h) pefloxacin (PF).

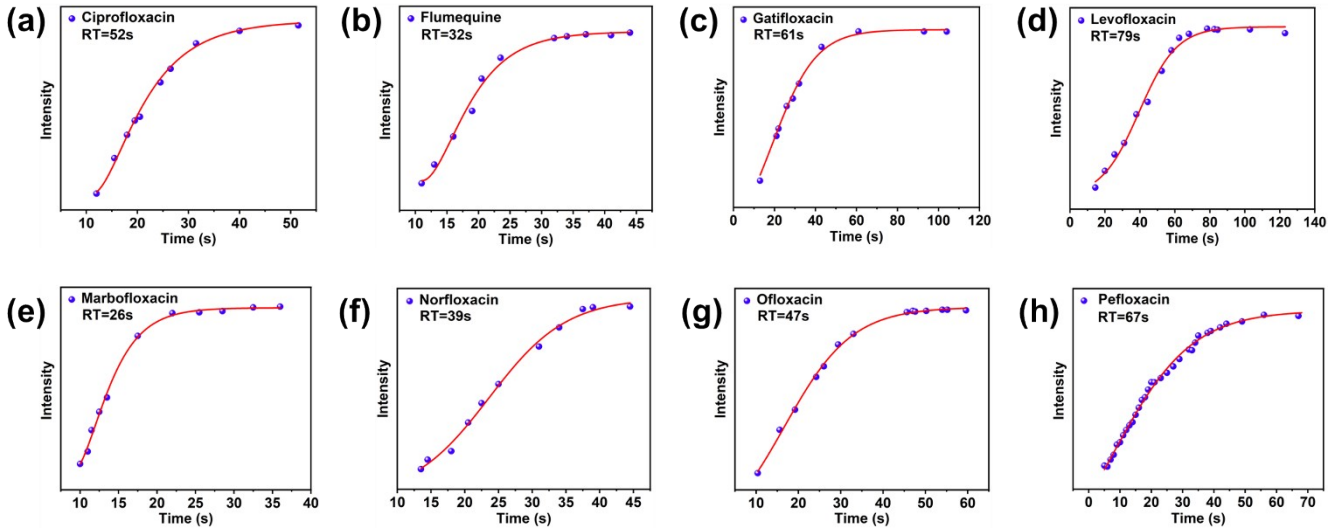

Fig. S11. Time-response emission spectra at 616 nm (excited at 323 nm) of **1** upon addition of 10^{-3} M eight QNs. (a) ciprofloxacin (CF): RT = 52 s, (b) flumequine (FQ): RT = 32 s, (c) gatifloxacin (GF): RT = 61 s, (d) levofloxacin (LF): RT = 79 s, (e) marbofloxacin (MF): RT = 26 s, (f) norfloxacin (NF): RT = 39 s, (g) ofloxacin (OF): RT = 47 s and (h) pefloxacin (PF): RT = 67 s. (RT: response time)

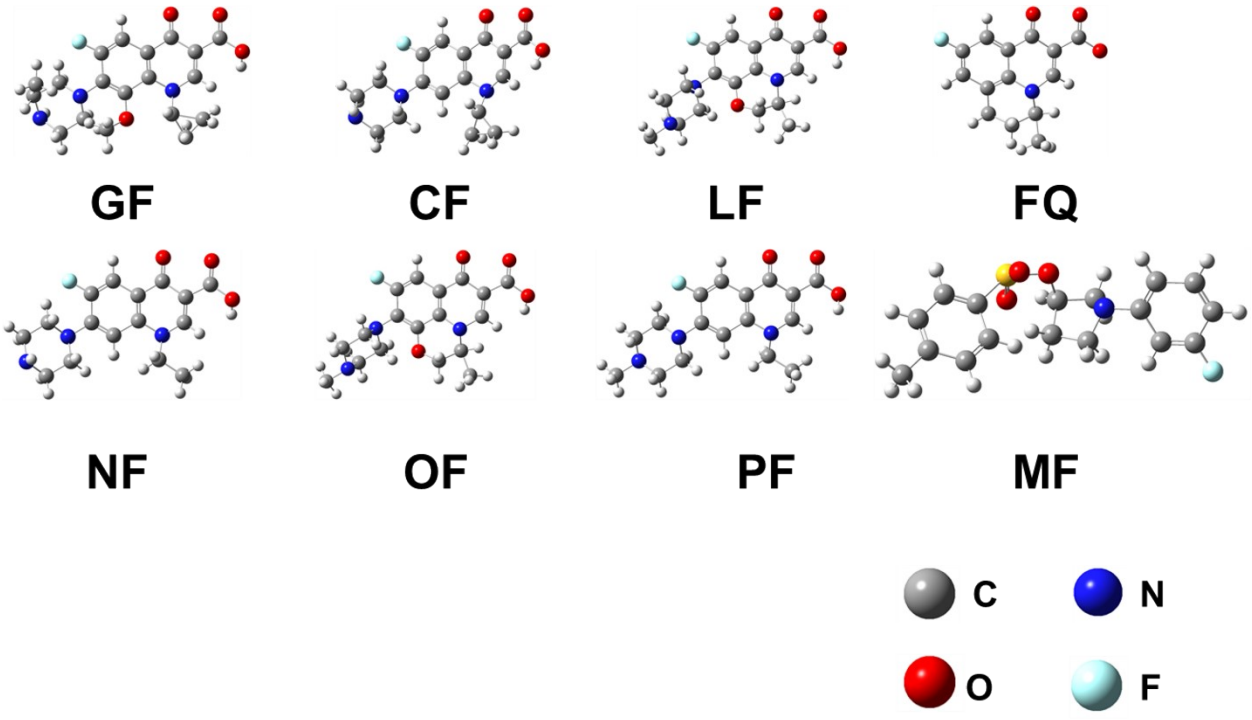

Fig. S12. The chemical structural formula of eight QNs.

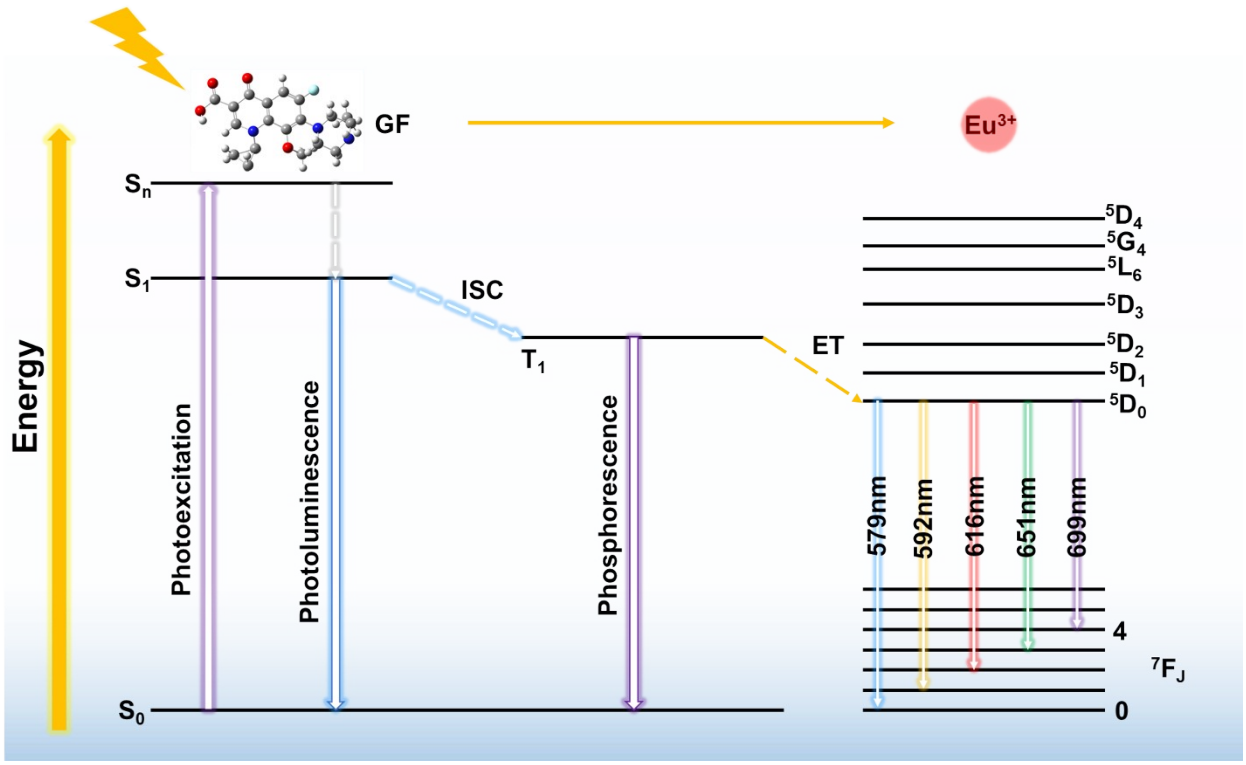

Fig. S13. Schematic diagram for the fluorescence response of **1** toward QNs mechanism. (ISC: intersystem crossing; ET: energy transfer)

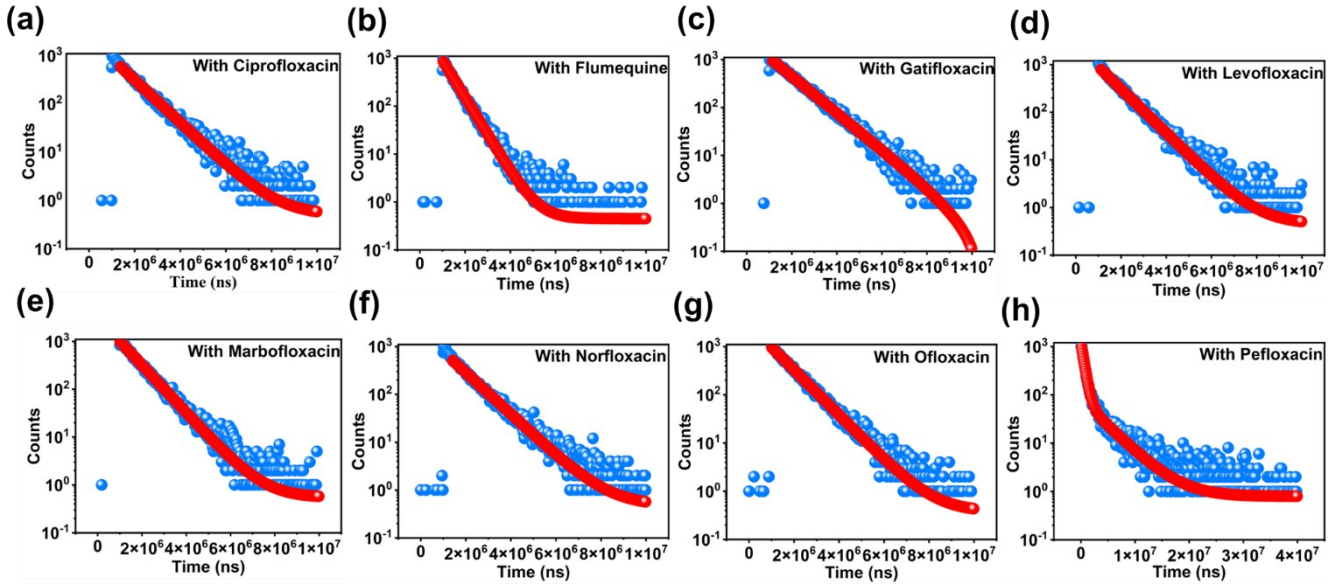

Fig. S14. Decay lifetimes of emission peak of 616 nm (Eu^{3+} $^5D_0 \rightarrow {}^7F_2$ transition) for **1** with 10^{-3} M eight QNs. (a) ciprofloxacin (CF), (b) flumequine (FQ), (c) gatifloxacin (GF), (d) levofloxacin (LF), (e) marbofloxacin (MF), (f) norfloxacin (NF), (g) ofloxacin (OF) and (h) pefloxacin (PF).

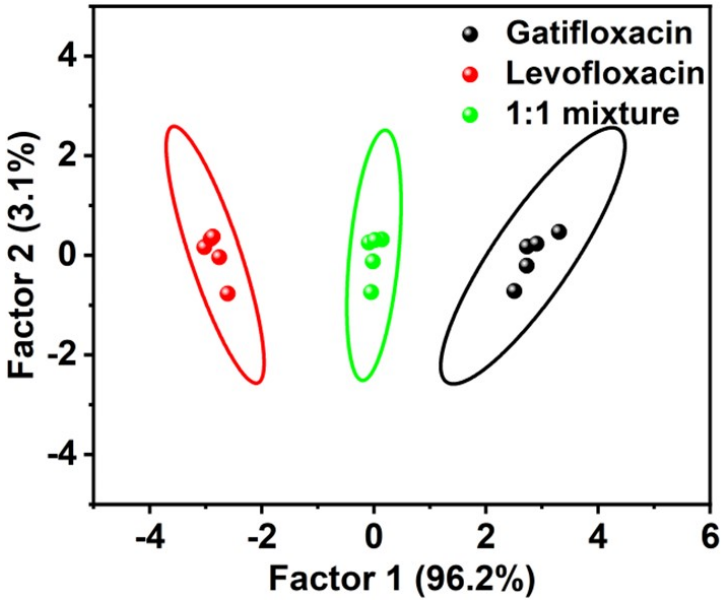

Fig. S15. Canonical 2D score plot for response patterns as obtained from PCA for 10^{-3} M LF、GF and 1:1 mixture of LF and GF. Ellipses represent 95% confidence.

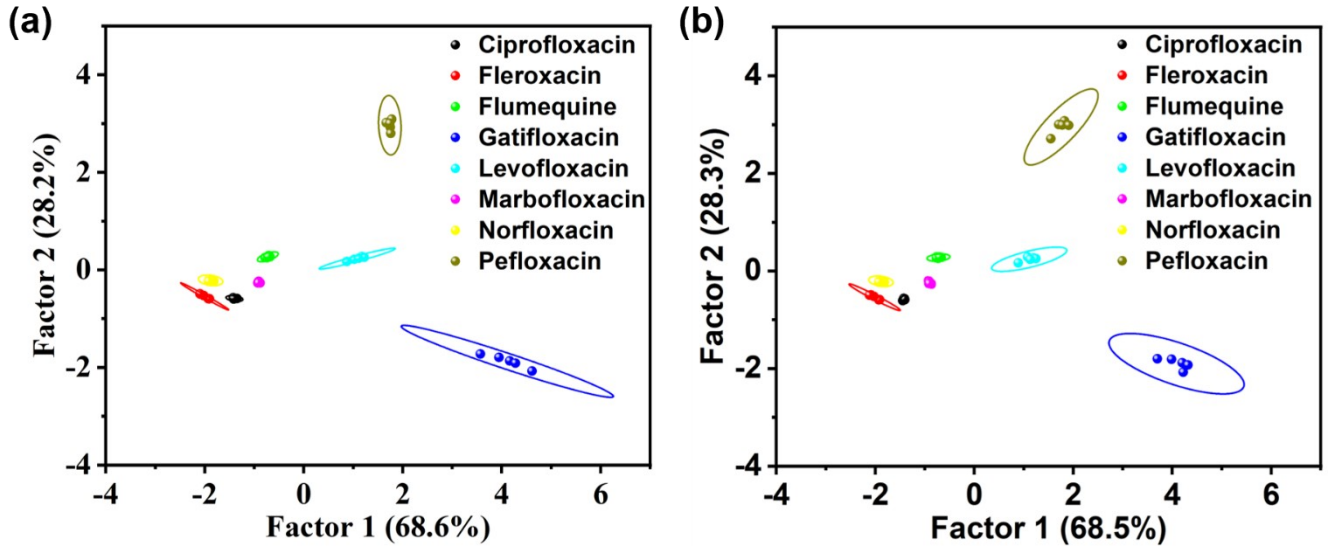

Fig. S16. Canonical 2D score plot for response patterns as obtained from PCA for eight QNs at 10^{-3} M in various components in (a) urine and (b) serum system (λ_{ex} = 323 nm). Ellipses represent 95% confidence.

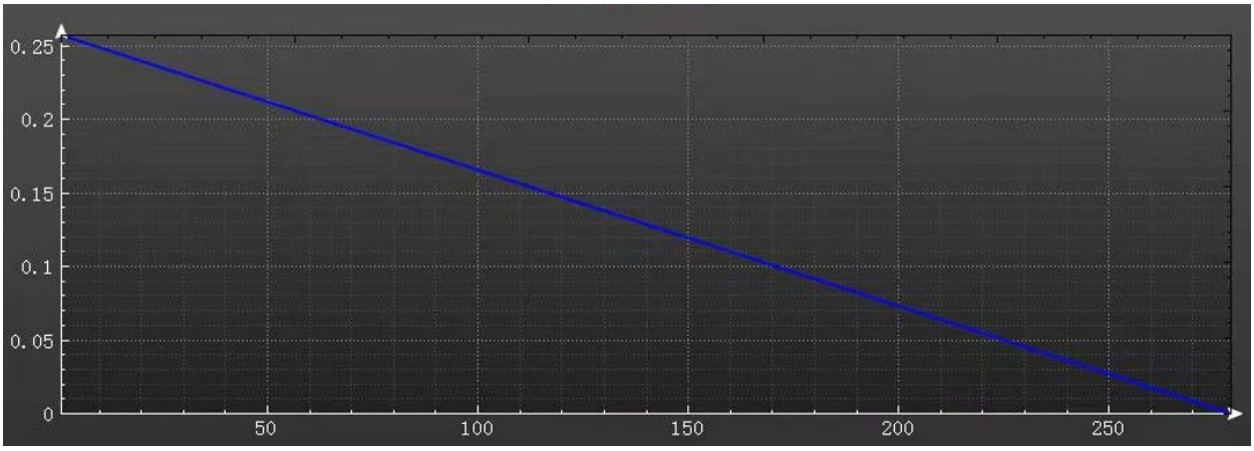

Fig. S17. Network training curve of the BPNN. Horizontal axis: Epoch; Vertical axis: Training MSE

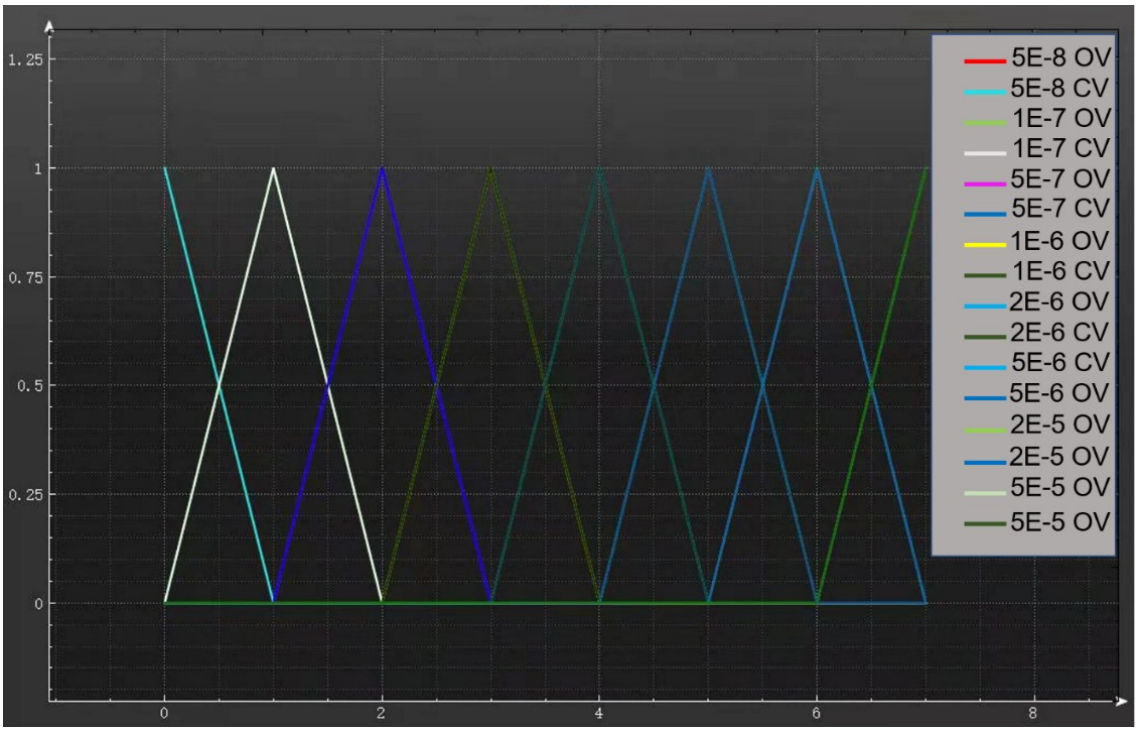

Fig. S18. Deviation curve of the BPNN (OV: original value; CV: calculated value). Horizontal axis: Eight concentrations of input items; Vertical axis: Training MSE.

Table S1. Element contents of C, N, O, S in EDX energy spectrum HOF-GS-10 and C, N, O, S, Eu in EDX energy spectrum **1**.

Element	Weight percentages (%)		Atomic percentage (%)	
	HOF-GS-10	Eu@HOF-GS-10	HOF-GS-10	Eu@HOF-GS-10
C	48.40	33.14	57.04	56.79
N	17.96	2.42	18.15	3.50
O	17.51	21.51	15.48	27.57
S	16.14	12.40	7.13	8.02
Eu	-	30.52	-	4.12
Total	100	100	100	100

Table S2. The relative values of the CIE chromaticity diagram of **1** mixed with eight QNs.

CIE chromaticity diagram		
Serial number	**Compounds**	**CIE**
(1)	Blank	(0.5992, 0.3356)
(2)	Flumequine	(0.2852, 0.1341)
(3)	Norfloxacin	(0.2232, 0.1175)
(4)	Pefloxacin	(0.1589, 0.0729)
(5)	Marbofloxacin	(0.3747, 0.3546)
(6)	Ofloxacin	(0.2588, 0.3058)
(7)	Levofloxacin	(0.2908, 0.3178)
(8)	Gatifloxacin	(0.3498, 0.2694)
(9)	Ciprofloxacin	(0.3617, 0.1985)

Table S3. Summary of fluorescence sensing parameters of **1** for detecting eight QNs in ethanol System.

Drug	Concentration range	Linear relationship	K_{EC}（mM）	R^2	Detection limit (mg L^{-1})
NF	10^{-7} - 10^{-5}	y = 6 ×10^9 x - 170.29	711.56	0.995	0.00782
OF	10^{-7} - 10^{-5}	y = 2 ×10^9 x + 3804.9	273.87	0.998	0.0265
CF	5×10^{-8} - 10^{-5}	y =7 × 10^9 x + 486.69	965.93	0.9949	0.00695
LF	5×10^{-8} - 10^{-5}	y = 2 × 10^9 x + 1166.5	238.67	0.9992	0.0265
MF	5×10^{-8} - 10^{-5}	y =4 × 10^9 x + 2272.3	421.91	0.9987	0.0133
PF	5×10^{-8} - 10^{-5}	y = 4 × 10^9 x + 2402.3	526.68	0.9921	0.0122
GF	5×10^{-8} - 5×10^{-5}	y = 3 × 10^9 x + 5154.8	352.01	0.9978	0.0184
FQ	5×10^{-8} - 5×10^{-6}	y = 2 × 10^9 x + 709.32	117.72	0.9915	0.0192

Table S4. Summary of the methods for sensing FQ.

method	LOD (mg L^{-1})	K_{EC} (mM^{-1})	Ref
Fluorescence detection (Ln@MOF)	0.0723	167.98	[S1]
Fluorescence detection (Ln@HOF)	0.114	-	[S2]
Plate diffusion (Yersinia spp. Strain)	0.1	-	[S3]
Biomimetic enzyme-linked immunosorbent assay	0.141	-	[S4]
Chiral liquid chromatography-tandem mass spectrometry	0.015	-	[S5]
Chiral liquid chromatography	0.016	-	[S6]
Liquid chromatography-electron spray ionization mass spectrometry	0.151	-	[S7]

Reference

[S1] S. Li, Y. Li, B. Yan, *CrystEngComm*, 2021, **23**, 5345-5352.

[S2] X. Xu, J. Wang, B. Yan, *Adv. Funct. Mater.*, 2021, **31**, 2103321.

[S3] P. Navrátilová, J. Vyhnálková, L. Vorlová, *J. Vet. Res.*, 2017, **61**, 467-472.

[S4] W. Liu, J. Wang, W. Yu, X. Wang, *Food Anal. Methods*, 2020, **13**, 403-411.

[S5] S. Li, B. Liu, M. Xue, J. Yu, X. Guo, *Chirality*, 2019, **31**, 968-978.

[S6] Y.-F. Wang, X.-F. Gao, H.-X. Jin, Y.-G. Wang, W.-J. Wu, X.-K. Ouyang, *Chirality*, 2016, **28**, 649-655.

[S7] Z. H. Hu, Y. G. Wang, H. X. Jin, X. K. Ouyang, W. J. Wu, *Chirality*, 2016, **28**, 737-743.

Table S5. Summary of fluorescence decay lifetime of **1** in ethanol (ET), **1** powder and **1** mixed with eight QNs at 298 K.

Sample	λ_{ex} (nm)	λ_{em} (nm)	τ_1 (μs)	A_1	Percentage (%)	τ_2 (μs)	A_2	Percentage (%)	τ^* (μs)	χ^2
1 in ET	323	616	371.48	330.92	100					1.001
1 Powder	323	616	385.04	1100.18	100					1
1-FQ	323	616	558.89	878.35	100					0.997
1-MF	323	616	871.8	1002.75	100					1.38
1-OF	323	616	927.22	963.35	100			—		1.122
1-LF	323	616	935.68	807.11	100					1.379
1-CF	323	616	983.19	598.42	100					1.469
1-NF	323	616	997.86	518.75	100					1.266
1-GF	323	616	1129.65	953.87	100					1.256
1-PF	323	616	563.81	1002.4	64.91	3987.98	76.63	35.09	1765.54	1.196

$[\tau^* = (A_1\tau_1^2+A_2\tau_2^2)/(A_1\tau_1+A_2\tau_2)]$

Table S6. Summary of input and output information during the training of BPNN for GF concentrations detection.

Input	Output							
I/I_0	5×10^{-8} M	1×10^{-7} M	5×10^{-7} M	1×10^{-6} M	2×10^{-6} M	5×10^{-6} M	2×10^{-5} M	5×10^{-5} M
1.12425	1	0	0	0	0	0	0	0
1.62626	0	1	0	0	0	0	0	0
3.33199	0	0	1	0	0	0	0	0
4.10211	0	0	0	1	0	0	0	0
5.64889	0	0	0	0	1	0	0	0
11.4487	0	0	0	0	0	1	0	0
29.5322	0	0	0	0	0	0	1	0
69.2656	0	0	0	0	0	0	0	1

In Table S6, all data is applied for training the BPNN. The I/I_0 values at 616 nm of every GF concentration as input information are inputted in the input column of the BPNN. Various "0" and "1" inputted into the output column of the BPNN, in which "0" represents the false GF concentration, and "1" represents the correct GF concentration. All data is used to train the BPNN.

Table S7. Network structure information.

Network structure information				
Input layer	1 neurons	1 Paranoid		
Hidden layer 1	6 neurons	1 Paranoid		
Hidden layer 2	6 neurons	1 Paranoid		
Hidden layer 3	6 neurons	1 Paranoid		
Output layer	8 neurons			
Network type	FANN_NETTYPE_LAYER			
Training function	FANN_TRAIN_RPROP			
Error function	FANN_ERRORFUNC_LINEAR			
Termination function	FANN_STOPFUNC_MSE			
Hidden layer excitation function	FANN_SIGMOID_SYMMETRIC			
Output layer excitation function	FANN_SIGMOID_SYMMETRIC			
Network weight value				
Arrangement	Wire number	Output point (n)	Input point (m)	Weight value (W)
1	0	0	2	-0.0889867
	1	1	2	0.484308
	2	0	3	0.688136
	3	1	3	-0.166992
	4	0	4	0.705895
	5	1	4	0.575009
	6	0	5	2.01062
	7	1	5	0.366775
	8	0	6	0.728024
	9	1	6	0.691508
	10	0	7	0.690002
	11	1	7	0.678255
	12	2	9	-0.395007
	13	3	9	0.559811
	14	4	9	1.19369
	15	5	9	0.010263
	16	6	9	1.13474
	17	7	9	0.569057
	18	8	9	-0.226494
	19	2	10	-0.21492
	20	3	10	0.677634
	21	4	10	1.92465
2	22	5	10	0.0486169
	23	6	10	1.16593
	24	7	10	-0.815626
	25	8	10	-0.159978
	26	2	11	0.396039
	27	3	11	0.75535
	28	4	11	3.97776
	29	5	11	1.14153
	30	6	11	26.5029
	31	7	11	608.978
	32	8	11	1.71353

	33	2	12	0.0955819
	34	3	12	1.2952
	35	4	12	67.2629
	36	5	12	1.17687
	37	6	12	230.436
	38	7	12	30.8023
	39	8	12	2.32355
	40	2	13	-0.0917954
	41	3	13	0.623873
	42	4	13	25.2375
	43	5	13	0.0198081
	44	6	13	13.4625
	45	7	13	4.27035
	46	8	13	-0.111031
	47	2	14	-0.103488
	48	3	14	0.695615
	49	4	14	1.38954
	50	5	14	-0.138719
	51	6	14	1.59029
	52	7	14	-0.0399597
	53	8	14	-0.101403
	54	9	16	0.939571
	55	10	16	1.56291
	56	11	16	0.331996
	57	12	16	0.949294
	58	13	16	-3.36237
	59	14	16	0.808534
	60	15	16	2.57041
	61	9	17	1.51703
	62	10	17	1.58897
	63	11	17	1.03478
	64	12	17	2.99107
	65	13	17	9.0174
	66	14	17	1.30292
3	67	15	17	0.371097
	68	9	18	-0.233343
	69	10	18	-0.216328
	70	11	18	-0.973328
	71	12	18	-1.83077
	72	13	18	-0.391698
	73	14	18	-0.214747
	74	15	18	-0.0605006
	75	9	19	122.824
	76	10	19	108.874
	77	11	19	-0.846042
	78	12	19	0.991912
	79	13	19	1.1093
	80	14	19	19.3405
	81	15	19	-1500

	82	9	20	1.33649
	83	10	20	1.41384
	84	11	20	2.16705
	85	12	20	-1.92816
	86	13	20	1.27245
	87	14	20	0.801562
	88	15	20	-0.105515
	89	9	21	0.910961
	90	10	21	0.435861
	91	11	21	-0.426692
	92	12	21	-0.467539
	93	13	21	-0.34581
	94	14	21	0.460003
	95	15	21	-0.062001
	96	16	23	75.5869
	97	17	23	195.675
	98	18	23	167.497
	99	19	23	247.15
	100	20	23	9.55186
	101	21	23	1137.58
	102	22	23	29.5664
	103	16	24	-2.65559
	104	17	24	-6.2509
	105	18	24	28.7103
	106	19	24	4.00223
	107	20	24	43.2315
	108	21	24	21.7192
	109	22	24	-7.6881
	110	16	25	-7.15568
	111	17	25	-18.5733
	112	18	25	-3.11314
4	113	19	25	2.65863
	114	20	25	21.4741
	115	21	25	-16.853
	116	22	25	-12.0277
	117	16	26	-1.42526
	118	17	26	-12.8793
	119	18	26	-15.5003
	120	19	26	1.79055
	121	20	26	-17.6899
	122	21	26	-2.09541
	123	22	26	-17.9254
	124	16	27	-4.44654
	125	17	27	41.5712
	126	18	27	0.306322
	127	19	27	0.604404
	128	20	27	-54.6462
	129	21	27	24.7767
	130	22	27	-19.304

131	16	28	-40.5971
132	17	28	23.3047
133	18	28	-0.0346161
134	19	28	0.174518
135	20	28	-21.7797
136	21	28	-8.89355
137	22	28	-0.768783
138	16	29	-56.7186
139	17	29	2.63563
140	18	29	0.143866
141	19	29	0.115309
142	20	29	44.272
143	21	29	0.421034
144	22	29	-3.59557
145	16	30	-9.44276
146	17	30	3.25947
147	18	30	7.22379
148	19	30	14.6223
149	20	30	55.5271
150	21	30	46.493
151	22	30	-9.86686

Input / output column coefficients for manual calculation

Listing	Minimum	Maximum
I/I0	1.06803	72.9112
0.00000005M	0	1
0.0000001M	0	1
0.0000005M	0	1
0.000001M	0	1
0.000002M	0	1
0.000005M	0	1
0.00002M	0	1
0.00005M	0	1

Deviation statistics: mean variance

Listing	All rows	Calculation line	Test line
0.00000005M	0	0	0
0.0000001M	7.06113E-09	7.06113E-09	0
0.0000005M	3.57022E-09	3.57022E-09	0
0.000001M	1.67194E-08	1.67194E-08	0
0.000002M	1.6875E-12	1.6875E-12	0
0.000005M	1.20697E-07	1.20697E-07	0
0.00002M	5.18104E-07	5.18104E-07	0
0.00005M	6.90625E-12	6.90625E-12	0

Table S8. The summary of mean square error (MSE), original value (OV.), calculated value (CV.), variance (Var.).

Input item (I/I_0)		1.12425	1.62626	3.33199	4.10211	5.64889	11.4487	29.5322	69.2656
5×10^{-8} M (MSE=0)	OV.	1	0	0	0	0	0	0	0
	CV.	1	0	0	0	0	0	0	0
	Var.	0	0	0	0	0	0	0	0
1×10^{-7} M (MSE=7.06e-09)	OV.	0	1	0	0	0	0	0	0
	CV.	0.00002	0.999964	0.000163	0	0	0	0	0.000168
	Var.	4.000E-10	1.296E-09	2.657E-08	0	0	0	0	2.822E-08
5×10^{-7} M (MSE=3.57e-09)	OV.	0	0	1	0	0	0	0	0
	CV.	0	0.000029	0.99992	0.0001305	0	0	0.0000655	0.0000005
	Var.	0	8.410E-10	6.400E-09	1.703E-08	0	0	4.290E-09	2.500E-13
1×10^{-6} M (MSE=1.67e-08)	OV.	0	0	0	1	0	0	0	0
	CV.	0.000192	0	0.00007	0.999829	0.0002505	0	0	0
	Var.	3.686E-08	0	4.9E-09	2.924E-08	6.28E-08	0	0	0
2×10^{-6} M (MSE=1.69e-12)	OV.	0	0	0	0	1	0	0	0
	CV.	0.0000005	0	0	0	0.999999	0.0000035	0	0
	Var.	2.5E-13	0	0	0	1E-12	1.225E-11	0	0
5×10^{-6} M (MSE=1.21e-07)	OV.	0	0	0	0	0	1	0	0
	CV.	0	0	0	0	0.000272	0.999197	0.0004965	0
	Var.	0	0	0	0	7.43E-08	6.448E-07	2.465E-07	0
2×10^{-5} M (MSE=5.18e-07)	OV.	0	0	0	0	0	0	1	0
	CV.	0	0	0	0	0	0.000511	0.998138	0.0006455
	Var.	0	0	0	0	0	2.611E-07	3.467E-06	4.166E-07
5×10^{-5} M (MSE=6.91e-12)	OV.	0	0	0	0	0	0	0	1
	CV.	0	0	0	0	0	0	0.0000025	0.999993
	Var.	0	0	0	0	0	0	6.25E-12	4.9E-11

In Table S8, all data is utilized to test the BPNN. The I/I_0 values at 616 nm of every GF concentration as input information are inputted in the input column of the BPNN. Through the BPNN calculation, various values (0-1) can be outputted, in which the values close to "0" represents the false GF concentrations, the values close to "1" represents the correct GF concentrations. By comparing the OV. with CV., the variance (Var.) can be obtained, which suggests that the BPNN has a good accuracy for distinguishing GF concentrations.

Table S9. The summary of input and output information in real batch calculation during the test of BPNN.

Input data	Output data							
I/I_0	5×10^{-8} M	1×10^{-7} M	5×10^{-7} M	1×10^{-6} M	2×10^{-6} M	5×10^{-6} M	2×10^{-5} M	5×10^{-5} M
1.12425	1	1.98E-05	1.1E-12	0.00019	7.32E-07	0	0	0
1.62626	0	0.999963	2.9E-05	1.5E-08	0	0	0	2.8E-16
3.33199	0	0.000163	0.99992	7E-05	0	0	0	5.6E-17
4.10211	0	0	0.00013	0.99983	5.55E-17	0	0	0
5.64889	0	0	1.6E-14	0.00025	1	0.000272	0	0
11.4487	0	0	1.5E-07	9.5E-11	3.57E-06	0.999197	0.000511	0
29.5322	0	3.60E-11	6.5E-05	3.7E-14	5.33E-15	0.000497	0.998138	2.6E-06
69.2656	0	0.000168	5.2E-07	3.3E-16	1.67E-16	1.87E-14	0.000645	0.99999

In Table S9, all data is utilized to test the BPNN. The I/I_0 values at 616 nm of every GF concentration as input information are inputted in the input column of the BPNN. Through the BPNN calculation, various values (0-1) can be acquired, in which the values close to "0" represents the false GF concentration, and the values close to 1 represents the correct GF concentration.